Available online at www.sciencedirect.com
ScienceDirect
Journal of Nuclear Materials 360 (2007) 304–314
journal of nuclear materials
www.elsevier.com/locate/jnucmat

In-pile electrochemical measurements on AISI 304 and AISI 306 in PWR conditions – Experimental results

R.W. Bosch *, M. Wéber, M. Vankeerberghen

SCK•CEN (Belgian Nuclear Research Centre), Department Reactor Materials Research, Boeretang 200, B-2400 Mol, Belgium

Received 31 March 2006; accepted 8 November 2006

Abstract

In-pile electrochemical measurements were performed in order to investigate the effect of radiation on the electrochemical corrosion behaviour of AISI 304 and AISI 316 in PWR primary water (400 ppm B and 2 ppm Li) at 300 °C. The corrosion potential was continuously monitored during the whole irradiation period. Polarization resistance measurements and electrochemical impedance spectroscopy were performed at regular intervals. Polarization curves were recorded halfway through and at the end of each reactor cycle. All measurements were performed on both an in-flux and an out-of-flux 3-electrode electrochemical cell, each containing a platinum high-temperature reference electrode and an yttrium-stabilized zirconia (YSZ) reference electrode. The results show a small influence of radiation on the corrosion potential. However, the impedance data show a marked difference between in-flux and out-of-flux. The Nyquist diagram shows one semi-circle and one flattened semi-circle of which a branch leaps off indicating an R-(R//C)-(CPE//RW) type equivalent circuit.

1. Introduction

Stainless steel AISI 304 and AISI 316 are extensively used as a structural material in the core of light water reactors. As these nuclear power plants age the stainless steel core components suffer from increasing irradiation damage e.g. their microchemistry and microstructure changes. As a result, irradiation assisted stress corrosion cracking (IASCC) has been occurring. In BWRs this type of cracking is strongly affected by the electrochemical potential [1–3]. IASCC is the interplay between a stressed material and its environment, i.e. both the material and the environment are influenced by radiation. The effect of radiation on materials results in changing material properties (e.g. increasing hardness and radiation-induced segregation), which makes them more susceptible to cracking. Radiation also causes radiolysis in the water resulting in a different water chemistry (e.g. local production of hydrogen peroxide increasing the oxidizing power of the water). Here we explore the possible influence of radiation on the electrochemical behavior of the stainless steels under representative PWR conditions, i.e. 400 ppm boron, 2 ppm lithium, 25 cc H_2/kg (STP) and 300 °C. This research can be seen as a continuation of the corrosion of fusion materials (COFUMA) experiment, where the effect of radiation on the electrochemical behaviour of AISI 316 L(N) IG and EUROFER 97 was investigated in

* Corresponding author.
E-mail address: rbosch@sckcen.be (R.W. Bosch).

0022-3115/$ - see front matter © 2006 Elsevier B.V. All rights reserved.
doi:10.1016/j.jnucmat.2006.11.002

demineralised water at atmospheric pressure and lower temperature [1]. A literature overview on the effect of radiation on the electrochemical behavior of materials has been given in the latter reference and specific effects are given in [2–7].

The objective of this research is to investigate the effect of radiation on the electrochemical corrosion behaviour of AISI 304 and AISI 316 under representative PWR conditions. Possible effects that can be distinguished are [2–7]:

- Radiolysis, that causes a change in water chemistry.
- An increase in temperature due to γ-heating of the stainless steels components.
- A direct flux effect, also known as the Compton effect [7]. Neutron radiation produces electrons in the stainless steel components, introducing an extra cathodic current.

Immediately it is obvious that when measuring the electrochemical parameters, the results lump all of these effects (see also [1]). This does not prevent us to perform qualitatively good measurements, but entails that the analysis will yield a global system response. It will be difficult, unless by modelling various processes independently (if this is at all possible) to get at specific effects. It is also an in-situ experiment without the possibility for direct observations apart from the electrochemical measurements, which is the major reason for attempting these measurements.

To carry out this investigation an experimental device has been designed named corrosion of fission materials (COFIMA). In it electrodes have been mounted at in-flux and out-of-flux positions. Two types of reference electrodes (Pt-electrode and YSZ-electrode) have been mounted as well at both positions. Electrochemical tests like electrochemical potential (ECP), linear polarization resistance (LPR) and electrochemical impedance spectroscopy (EIS) have been carried out at identical electrodes at the two different positions. This should allow to elucidate the global effect of radiation of the electrochemical behaviour on the stainless steel electrodes.

2. Experimental

2.1. Experimental set-up

The experiments were carried out in the third leg (IPS3) of a PWR loop (CALLISTO) [8] in the BR2 material test reactor. Table 1 shows typical characteristics for IPS3. In IPS3 a rig allows for the proper mounting of the electrodes, their signal cables and an electrical-feed-through system leading signal cables out of the experiment to the measurement equipment, which is about 10 m away [9]. Figs. 1

Table 1
Characteristics for IPS3 of the PWR loop CALLISTO

Nuclear data	
Thermal flux	$0.9–1.0 \times 10^{14}$ n/cm^2/s
Thermohydraulic data	
Temperature	295–305 °C
Pressure	150–157 bar
Flow rate	±1.1 kg/s
Chemical data	
Boric acid	400 ppm B
Lithium hydroxide	±2 ppm Li
pH	±7.0 (25 °C) and ±7.3 (300 °C)
Hydrogen variations	20–36 cc H_2(STP)/kg

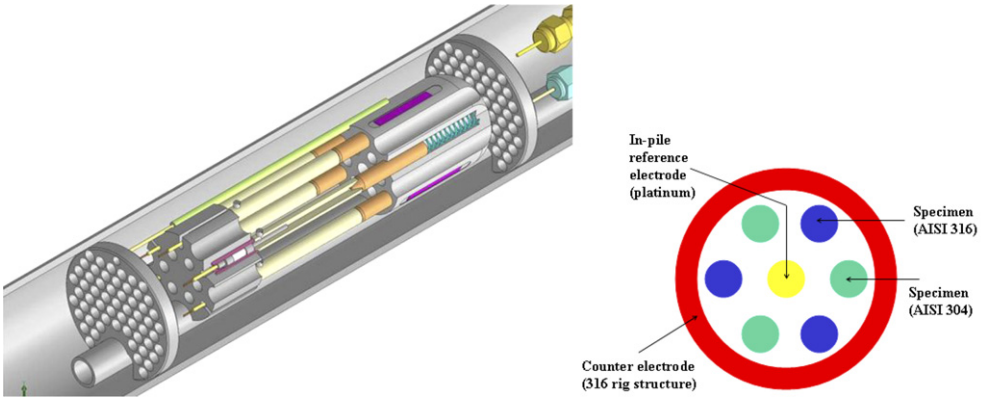

Fig. 1. 3D drawing and cross section of the in-flux section of the COFIMA rig (a similar section exist out-of-flux).

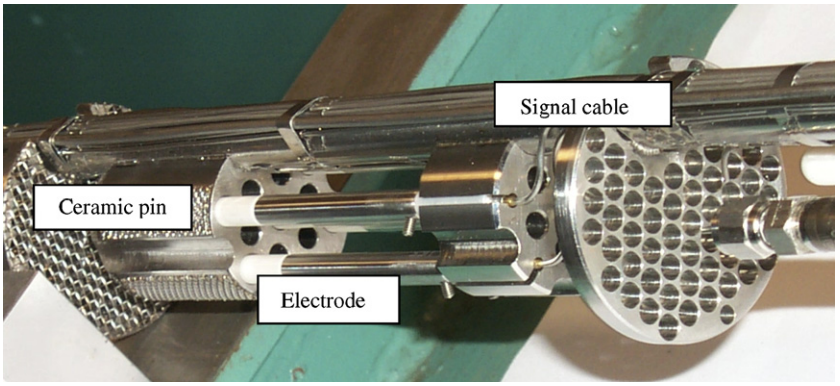

Fig. 2. In-flux section of the COFIMA rig showing the position of the electrodes, ceramic pins and the mineral-insulated signal cable.

and 2 show the arrangement of the COFIMA electrodes. The in-flux and out-of-flux sections each contain two specimens made of AISI 304, two specimens made of AISI 316 and a central platinum reference electrode. All are of dimension diameter 5 mm by 5 cm length (surface area 6.83 cm^2) and are connected to mineral-insulated signal cables with the aid of a special connector and are held into place by zirconium oxide parts to electrically insulate them from the frame. The out-of-flux section is positioned down-stream of the in-flux section at a distance of about 1 m. Fig. 3 shows a schematic of the assembly inside the PWR loop. Notice that the signal cables have to cross a long distance (about 10 m) before they reach the measuring equipment. The long leads give rise to a stray capacitance (≈5 nF) and resistance (≈80 Ω). These values could have a small influence on the impedance measurements depending on the impedance of the system under investigation and the perturbation frequency.

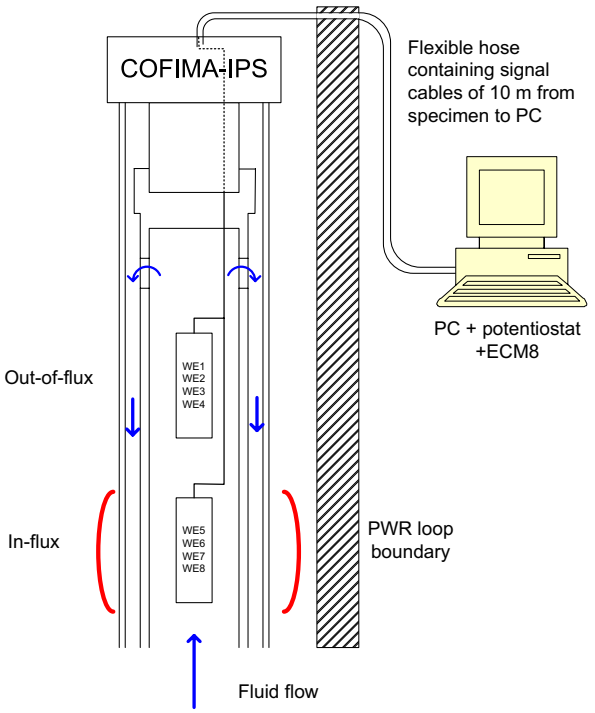

Fig. 3. Schematic of the electrode assembly in the PWR loop.

2.2. Electrochemical measurements

The electrochemical measurements were performed in a standard three-cell electrode arrangement. The platinum reference electrodes (PRE) are located in the centre of the test sections, assuring symmetry. The 316 stainless steel structure of the rig is used as counter electrode. The specimens are located around the PRE and are electrically insulated from the rig structure by ceramic pins. One mineral-insulated and shielded cable was connected to each of the specimen and the in-flux platinum reference electrode (IPRE). All the measurement cables were brought to a terminal block to which the measurement systems were branched. Open circuit potentials were measured at one minute intervals by an Agilent® data acquisition system. Specific electrochemical measurements were controlled by a multiplexed GAMRY® potentiostat system (PC4-300 and ECM8). The ECM8 electrochemical multiplexer performs one measurement at a time for each electrochemical cell, leaving the others disconnected. Fig. 4 shows the assembly of the potentiostat and multiplexer for four electrochemical cells. In reality there are 8 electrochemical cells. They all share the counter and a influx or out-of-flux reference electrode. At regular intervals the electrochemical system performed corrosion potential (E_{corr}, every

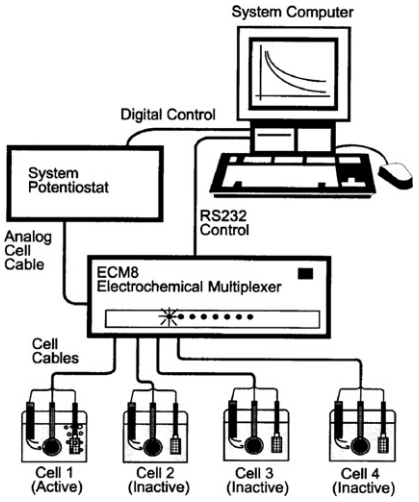

Fig. 4. Potentiostat and muliplexer.

minute), polarisation resistance (R_p, every hour) and electrochemical impedance spectroscopy (EIS, every day) measurements. At a few intervals, i.e. at the end of a testing campaign for the measurement is destructive, polarisation curves were recorded. The polarisation resistance was determined with the linear polarization resistance (LPR) technique. The potential was scanned from −10 mV to +10 mV against the open circuit potential with a scan rate of 0.5 mV/s and a sampling time of 2 s. EIS was performed from 10 kHz to 10 mHz (10 points per decade) with a perturbation amplitude of 10 mV RMS around the open circuit potential. Polarisation curves were measured from −1 V to +2 V against the open circuit potential with a scan rate of 600 mV/h (ASTM G 5-94) and a sampling time of 10 s. The potential of the in-flux platinum reference electrode (IPRE) has been measured continuously against the potential of the out-of-flux platinum reference electrode (OPRE).

3. Results

3.1. Corrosion potential

A huge amount of data has been collected during the various test campaigns. The following graphs will give a summary of the first results of the tests carried out with the stainless steel 304 electrodes. Fig. 5 shows the temperature of the in-flux and out-of-flux electrodes. The temperature rise (due to γ-heating) at day 2 indicates the start of the reactor. Initially the loop is at hot standby (±250 °C). Fig. 6 shows the ECP values. The ECP values are very similar and only a minor difference between the in-flux and out-of-flux electrodes can be noticed. The mean value of about −780 mV SHE is close to the hydrogen water chemistry potential at 300 °C.

3.2. Polarization resistance

Fig. 7 shows values of the polarization resistance obtained with LPR. There is a small shift in polarization resistance at the start of the reactor. This

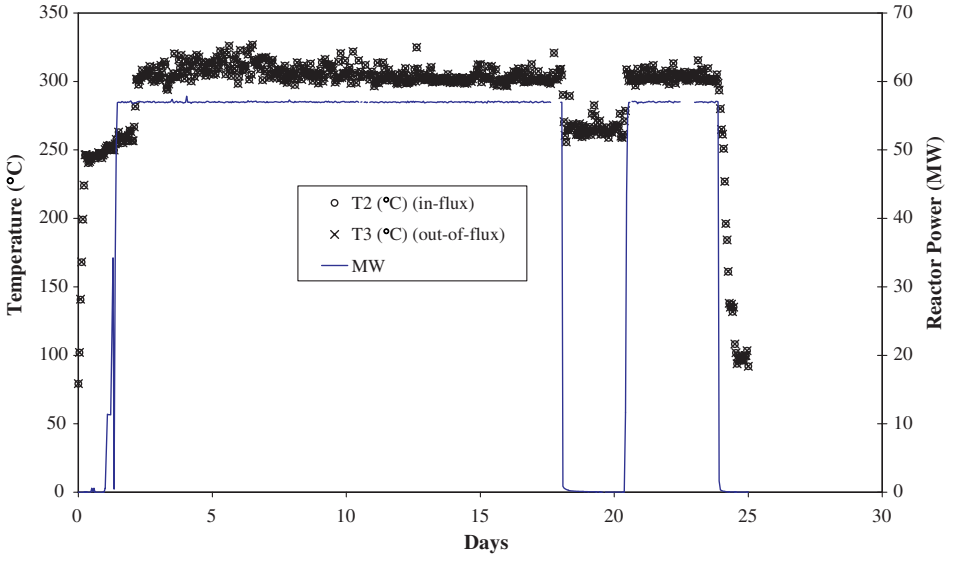

Fig. 5. Water temperature in the CALLISTO PWR loop in and out-of-flux. The distance between T2 and T3 is approximately 1 m.

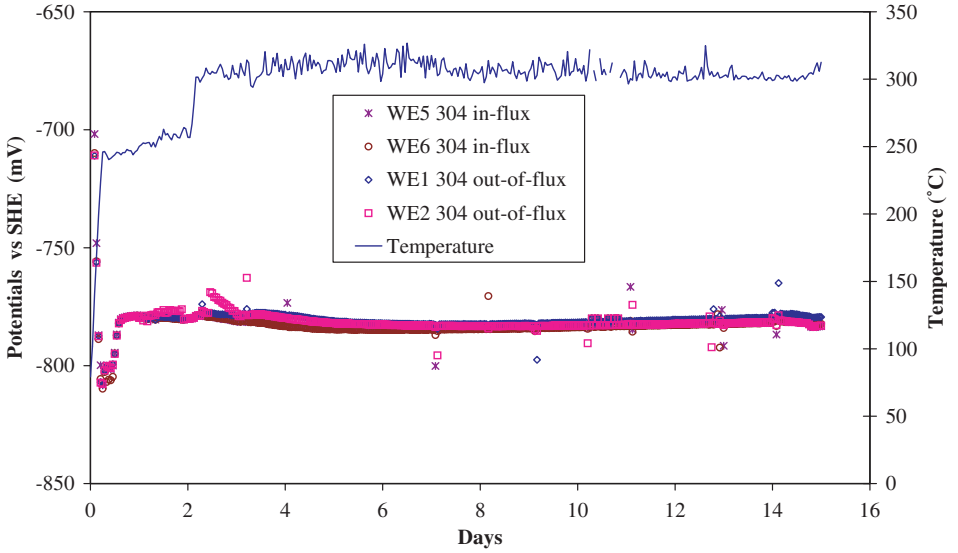

Fig. 6. ECP values of stainless steel 304 in PWR-water at 300 °C.

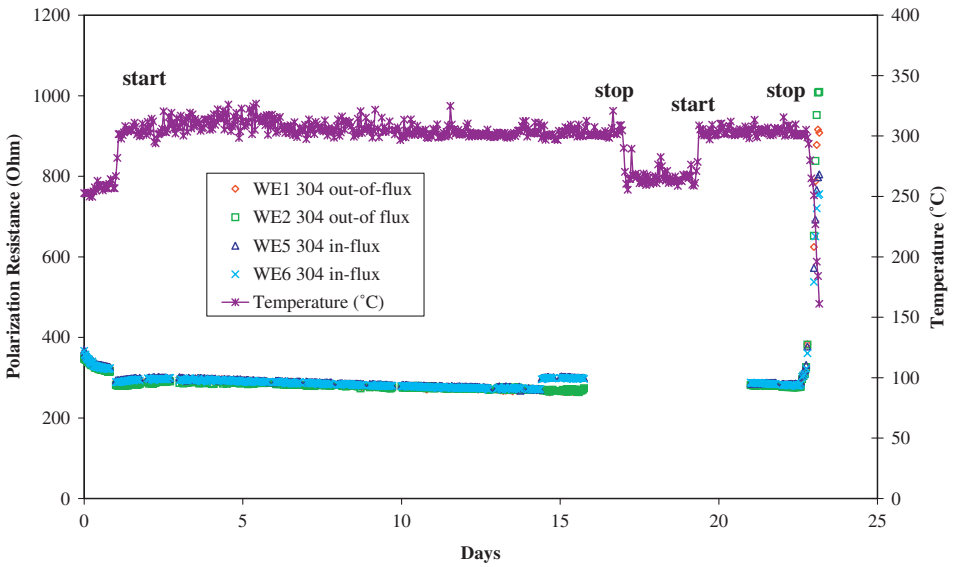

Fig. 7. Polarization resistance of stainless steel 304 in PWR-water at 300 °C.

shift is however similar for the in-flux and out-of-flux electrode and so only related to the temperature increase. A small difference between the in-flux and out-of-flux polarization resistance is only observed once around day 15. No significant explanation could be found for this effect.

3.3. Electrochemical impedance

Fig. 8 shows the Nyquist diagrams obtained with EIS after two weeks of testing. A clear difference between the in-flux and out-of-flux electrodes can be noticed. The high frequency part is clearly shifted right upon irradiation. Here we believe that this can be related to a difference in the impedance of the oxide layer. This effect is opposite to the one observed in reference [1], where a decrease in the polarization resistance was observed with increasing radiation. This was related to an increase in temperature and radiolytic water chemistry change, as there was no hydrogen present to suppress the radiolysis. The stray capacitance and resistance of the

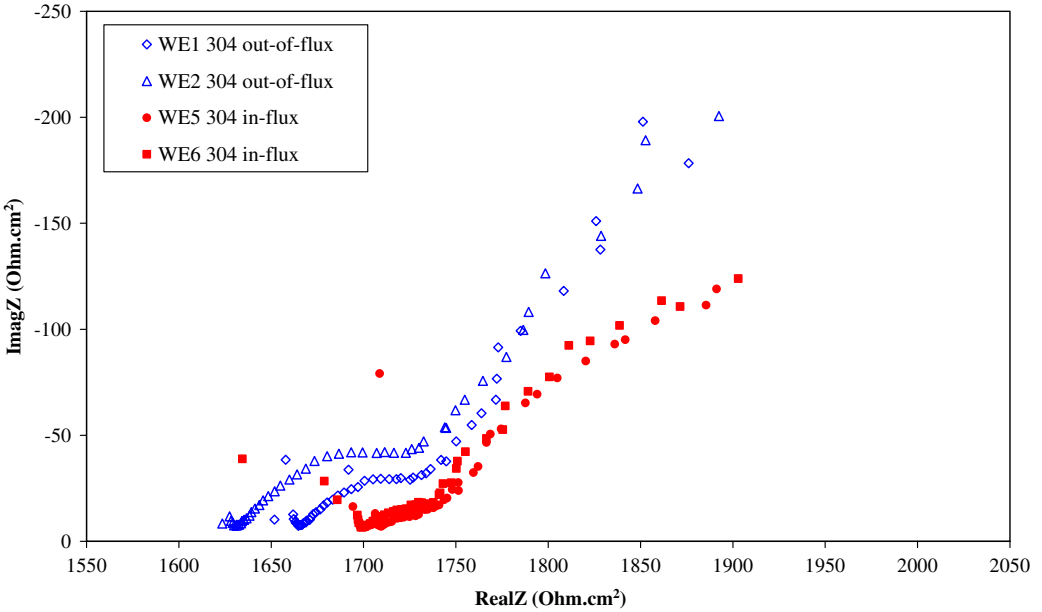

Fig. 8. Nyquist diagrams of EIS data of stainless steel 304 in PWR-water at 300 °C after 2 weeks of testing.

leads might give similar results depending on the perturbation frequency. For our system their influence can be neglected as at 10 kHz the contribution of the cable impedance is small. It is indeed possible that the in-flux oxide layer formed with radiation is different than the out-of-flux oxide layer. The intermediate and low frequency part is also different, suggesting that the electrochemical processes that take place at the metal-oxide–solution interface are slightly different or occur at a different rate. Due to the high flow rate (1–1.5 m/s) it is possible that oxidizing species formed at the in-core section do reach the out-of-flux electrodes. Hydrogen water chemistry however suppresses radiolysis and so it is

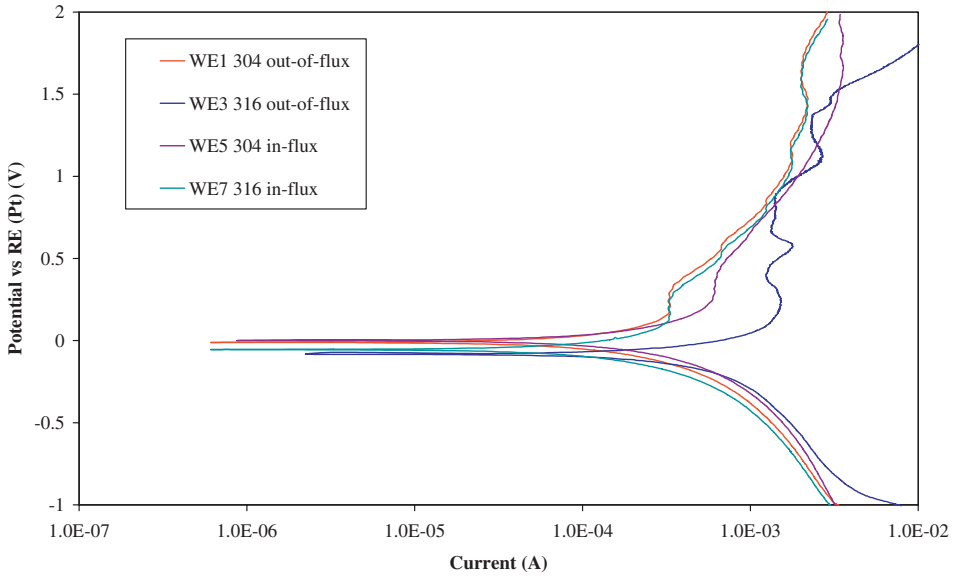

Fig. 9. Polarization curves of stainless steel 304 and 316 in PWR-water at 300 °C after 3 weeks of testing.

difficult to make a clear statement on this. A first modeling attempt based on an equivalent circuit will be presented in the next section.

3.4. Polarization curves

Fig. 9 shows polarization curves obtained after 3 weeks of exposure. All four polarization curves show a clear passive behavior with different oxidation–reduction peaks. These peaks can be related to transitions in oxide types. The differences between the in-flux and out-of-flux measurements are more pronounced for the 316 SS electrodes. The influence of radiation can however not be determined significantly from these measurements.

4. Discussion

4.1. Corrosion potential

A plausible explanation for the corrosion potential behaviour deduced from two in-pile experiments, corrosion of fusion materials (COFUMA) and corrosion of fission materials (COFIMA) is given below.

The COFUMA experiment was performed in a thimble tube filled with demineralised water and showed an increase in the corrosion potential with the neutron flux. The COFIMA experiment was performed in a PWR loop and showed that the long-term corrosion potential remained the same when a neutron flux was present but a slight decrease in corrosion potential was observed just after a neutron flux increase (Fig. 6). The decrease was short-lived and there was no long-term effect.

The results of both experiments can be tied together when (1) considering that in COFIMA radiolysis is suppressed by the presence of dissolved hydrogen – whilst in the COFUMA it is not – and (2) realizing that the first effect on the anodic reaction is an increase in current density due to gamma heating in the film and/or the Compton effect since both increase the transport rate through the passive oxide film.

Fig. 10 represents the various stages in this explanation. The left graphs show the out-of-flux situation. The corrosion potential is the potential for which the anodic and cathodic currents are equal. The middle graphs show the effect of the irradiation

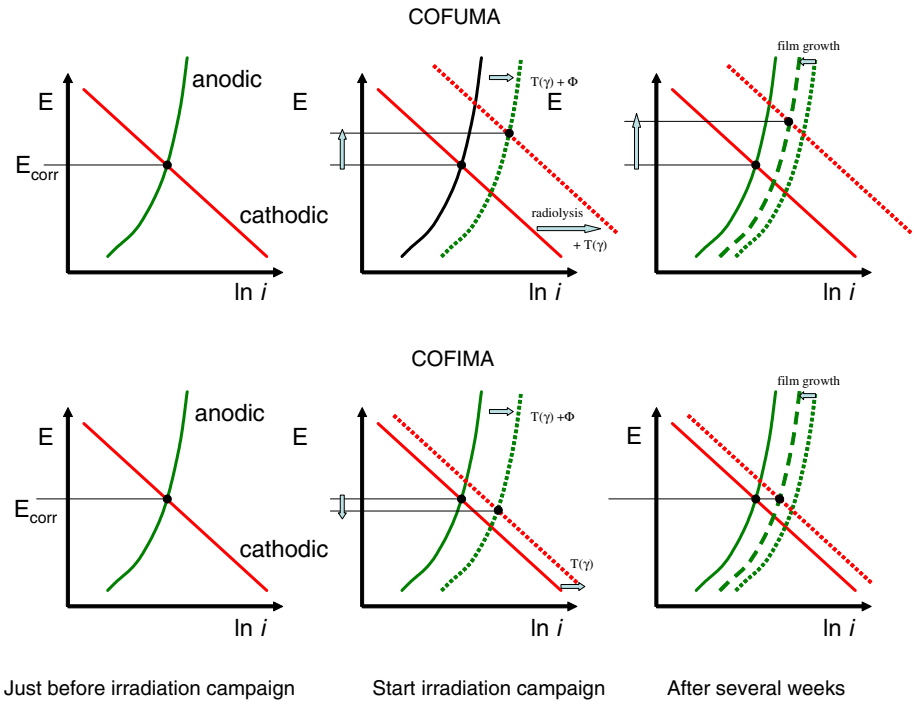

Fig. 10. Evans diagrams explaining the possible difference in ECP evolutions due to radiation between the COFUMA (pure water at 90 °C) and COFIMA (PWR-water 300 °C) irradiation experiments.

on the anodic and cathodic current density. The anodic current density increases due to a gamma flux related temperature increase and, possible, a Compton effect. The cathodic current density increases due to a gamma flux related temperature increase and, for COFUMA, a compositional change in the environment due to radiolysis. The net effect for the COFUMA experiment is a rise in the corrosion potential, whilst for the COFIMA experiment it is a drop in the corrosion potential. The right graphs show the long term effect on the corrosion potential. As a result of the irradiation the oxide film starts growing (see also analysis of the EIS results). This reduces the anodic current density and increases the corrosion potential. In the case of the COFUMA experiment the long-term corrosion potential shift is positive. In the case of the COFIMA experiment the initial drop in corrosion potential is compensated by oxide growth and there is no long-term irradiation effect on the corrosion potential.

4.2. Polarization measurements

The measured polarization resistances do not reflect a clear difference between in-flux and out-of-flux position. A hardly noticeable change can be seen at the start of the flux. This minimal increase is in agreement with the reasoning above i.e. that in the beginning a slight increase of the anodic current (=smaller polarization resistance) occurs. Also the polarization curves show clearly that the oxide layers are exactly the same for the in-flux and out-of-flux positions. This is reflected by the oxidation/reduction peaks (small humps) in the polarization curves. Notice that the sign of the derivative of the potential–current plot can be negative. This is usually attributed to the formation of an oxide layer (=passivation) or the formation of an adsorption layer.

4.3. A modelling attempt with the EIS data

The data interpretation will be carried out with a simple model based on an equivalent circuit (Fig. 11). The physical meaning of this equivalent circuit is based on the following assumptions:

- A rather thick (up to a few μms) oxide layer exists between the metal and solution [10–13]. This oxide layer can consist of a thin epitaxial spinel barrier layer and a thicker porous deposited spinel type layer [10,11]. In the equivalent circuit the whole oxide layer is represented by a capacitor (C_{ox}) and a resistance (R_{ox}), assuming that (part of) the oxide layer shows dielectric behaviour.
- The outer oxide layer has a rough and porous structure [10,12]. This is represented by a constant phase element (CPE) [14]. This CPE represents the distribution of charge (double layer capacity) over the surface area of the working

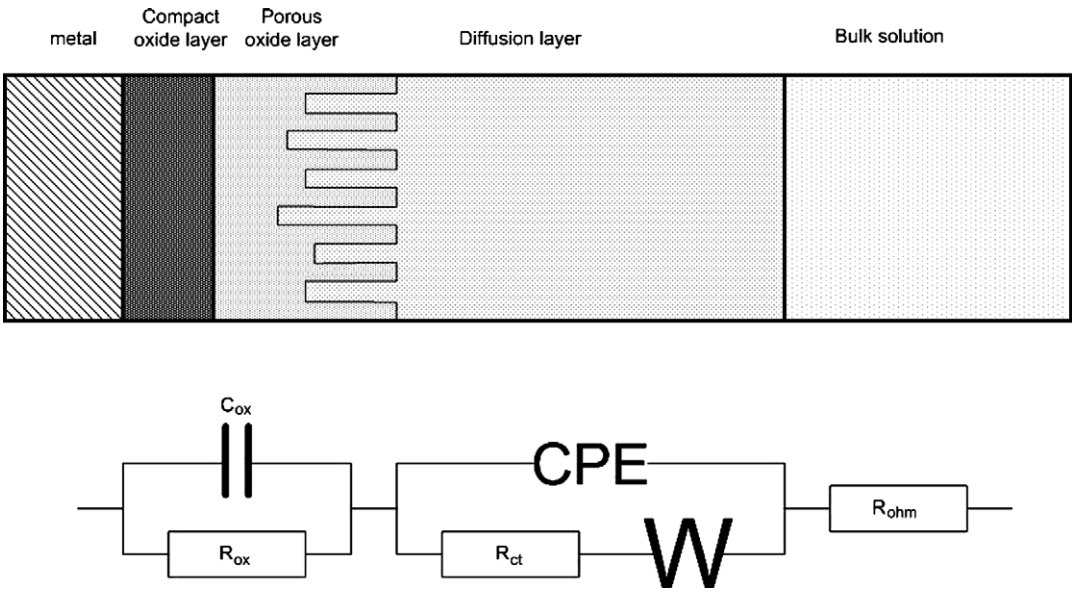

Fig. 11. Equivalent circuit representing the metal-oxide–solution interface.

electrode. A more elaborate modelling is possible with a transmission line approach [15–17], but that is outside the scope of this paper.

- The electrochemical behaviour at the oxide solution interface is represented by a charge transfer resistance (R_{ct}) and a Warburg impedance (W). The Warburg impedance describes the diffusion processes that happen at the interface [18]. A diffusion impedance arises when the surface concentration of an electrochemically active specie changes during the ac cycle.
- An ohmic resistance exists between the reference electrode and the electrochemical impedances. This ohmic resistance is related to the solution resistance of the electrolyte solution.

With this equivalent circuit model it is possible to extract the following physical parameters from the COFIMA impedance data. Based on the capacity of the oxide layer, it is possible to determine the oxide layer thickness when the relative electric permittivity is known. For chromium oxide a value of the relative electric permittivity of 12 can be found in literature [20]. The Warburg impedance can be used to have an estimate of the diffusion coefficient of one of the ions involved. Assume a simple redox system,

$$\mathrm{Ox} + \mathrm{ne}^- \Longleftrightarrow \mathrm{Red} \tag{1}$$

the Warburg impedance is then represented by [14,18],

$$\mathrm{W} = \frac{\sigma}{\sqrt{\omega}} - \mathrm{i}\frac{\sigma}{\sqrt{\omega}} \quad \text{with,} \tag{2}$$

$$\sigma = \frac{RT}{n^2F^2A\sqrt{2}}\left(\frac{1}{\sqrt{D_{\mathrm{Ox}}}C_{\mathrm{Ox}}} + \frac{1}{\sqrt{D_{\mathrm{Red}}}C_{\mathrm{Red}}}\right) \tag{3}$$

where σ is the so-called Warburg coefficient, D diffusion coefficient and C the concentration in mol/l. The Warburg coefficient can be obtained from the impedance modelling. Then one physical parameter can be obtained like the diffusion coefficient or concentration of one of the species. In our case (Eq. (3)) the simplified form of the Warburg impedance (diffusion layer thickness is assumed to be infinite) is used. This fits with the low frequency data as shown in the Nyquist plots i.e. a line with an angle of 45° with the real-axis.

The electrolyte resistance can be determined from the ohmic resistance as the whole set-up has been tested in a solution with known conductivity. The fit of all the impedance data have then been carried with Echem software from Gamry [19]. Results are summarized in Figs. 12 and 13 and in Tables 2 and 3. For each fit the 'Goodness of Fit' parameter is given as well. This parameter is calculated by the Echem software. A value of about 0.0001 means a good fit. The negative value of the ohmic resistance of WE5 should be discarded, due to the large uncertainty in the fit result of this parameter. This can be explained with Fig. 13, where it can be seen that there are only a few data points available for the fit of the high frequency semicircle. In Table 4 the cal-

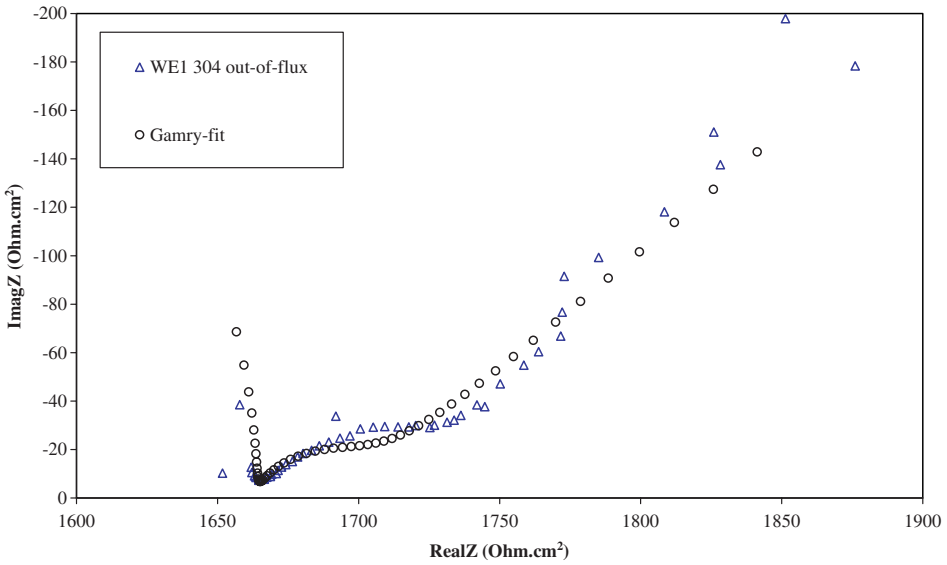

Fig. 12. Nyquist diagram of EIS data of stainless steel 304 (out-of-flux) in PWR-water at 300 °C after 2 weeks of testing.

Table 2
EIS fit results for WE1 and WE2 AISI 304 out-of-flux

	WE1 304 out	'+ -'	WE2 304 out	'+ -'
R_{ox}	95.91 Ω	70.38	133.7 Ω	172.7
C_{ox}	55.10 nF	82.72	24.40 nF	63.57
Y	5.292 mS s^{-n}	21.67	5.910 mS s^{-n}	11.47
n	0.8521	0.9661	0.8308	0.5282
W	106.9 mS $s^{-0.5}$	15.69	98.66 mS $s^{-0.5}$	13.99
R_{ct}	5.911 Ω	7.045	10.54 Ω	6.972
R_{ohm}	147.7 Ω	71.37	104.8 Ω	173.6
Goodness of fit	9.62E−05		9.08E−05	

Table 3
EIS fit results for WE5 and WE6 AISI 304 in-flux

	WE5 304 in	'+ -'	WE6 304 in	'+ -'
R_{ox}	443.9 Ω	1.784 k Ω	164.0 Ω	235.8 Ω
C_{ox}	2.493 nF	20.17 nF	18.67 nF	55.47 nF
Y	46.30 mS s^{-n}	148.9 mS	28.05 mS s^{-n}	66.52 mS
n	332.7 m	434.2 m	284.0 m	402.6 m
W	51.25 mS $s^{-0.5}$	151.2 mS	67.96 mS $s^{-0.5}$	77.55 mS
R_{ct}	7.134 Ω	25.89 Ω	11.13 Ω	9.269 Ω
R_{ohm}	−195.2 Ω	1.789 k Ω	80.82 Ω	242.7 Ω
Goodness of fit	1.29E−04		1.26E−04	

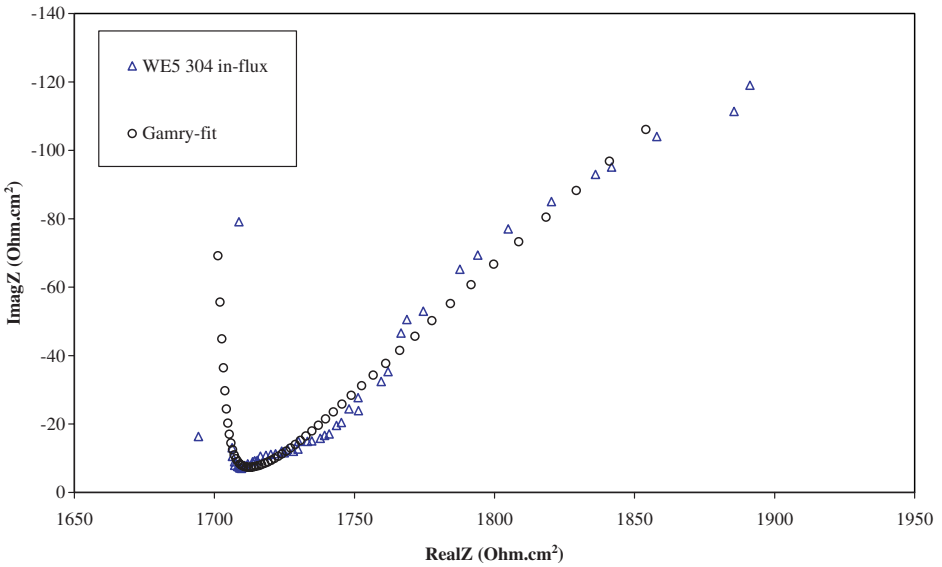

Fig. 13. Nyquist diagram of EIS data of stainless steel 304 (in-flux) in PWR-water at 300 °C after 2 weeks of testing.

Table 4
Comparison of the oxide layer thickness

	WE1 (out-of-flux)	WE2 (out-of-flux)	WE5 (in-flux)	WE6 (in-flux)
Oxide thickness (μm)	1.31 ± 0.87	2.97 ± 1.14	29.09 ± 3.59	3.88 ± 1.3

culated oxide layer thicknesses are presented. The electric permittivity for the oxide layer is taken from literature ($\varepsilon_r = 12$) [20]. Although the values may not be correct in an absolute sense, they clearly indicated a thicker oxide layer under irradiated conditions.

5. Conclusions

In-pile electrochemical measurements on stainless steel AISI 304 and AISI 316 electrodes have been carried out successfully in a PWR loop in the BR2 materials test reactor during a test campaign that lasted four weeks.

The differences between the electrode potentials and the polarisation resistances of the in-flux and out-of-flux stainless steel electrodes were small. Also the polarization curves did not differ significantly. A small but clear difference between in-flux and out-of-flux behaviour for EIS results could be obtained. This is assumed to be associated with small, but distinguishable differences in oxide layer structure and chemistry.

Based on the relative small values of the polarization resistances and impedances the electrochemical behaviour of the electrodes was assumed to be dominated by the electrokinetics of water and hydrogen.

References

[1] M. Vankeerberghen, R.W. Bosch, R. Van Nieuwenhove, J. Nucl. Mater. 312 (2003) 191.
[2] D.F. Taylor, Corrosion 47 (1991) 115.
[3] M.G. Danielson, Corrosion 51 (1995) 450.
[4] A.V.Bjalobzeskii, Korrosion durch Strahlung, EDV – Nr. 7614376, Printed in German Democratic Republic, 1970.
[5] P. Scott, J. Nucl. Mater. 211 (1994) 101.
[6] P. Scott, Corrosion 56 (2000) 771.
[7] M.E. Indig, J.L. Nelson, Corrosion 47 (1991) 202.
[8] M. Wéber, R.W. Bosch, L. Vermeeren, in: Proceedings of the International Conference on Water Chemistry of Nuclear Systems, San Francisco, October 2004.
[9] R.W. Bosch et.al., in: Proceedings of the International Conference on Water Chemistry of Nuclear Systems, San Francisco, October 2004.
[10] S.E. Ziemniak, M. Hanson, Corros. Sci. 44 (2002) 2209.
[11] M. Da Cunha Belo, M. Wallis, N.E. Hakiki, J. Corset, E. Picquenard, G. Sagon, D. Noël, Corros. Sci. 40 (1998) 447.
[12] M. Postler, R.W. Bosch, S. Van Dyck, in: International Conference on Environmental Degradation of Materials in Nuclear Power Systems – Water Reactor, Stevenson (US) 2003.
[13] V. Ignatova, M. Vankeerberghen, S. Gavrilov, R.-W. Bosch, S. Van Dyck, S. Van den Berghe, in: Proceedings of the Passivity-9, June 27–July 1 2005, Paris, France.
[14] J.R. Macdonald, Impedance Spectroscopy, Emphasizing Solid Materials and Systems, John Wiley, 1987.
[15] R. de Levie, Adv. Electrochem. Electrochem. Eng. 6 (1967) 329.
[16] D.D. Macdonald, Corrosion 46 (1990) 229.
[17] K. Jüttner, Electrochim. Acta 35 (1990) 1501.
[18] R. Cottis, S. Tyrgoose, Electrochemical Impedance and Noise, in: B.C. Syrett (Ed.), Corrosion Testing Made Easy, NACE International, 1999.
[19] Echem software, Gamry 2005.
[20] N.E. Hakiki, S. Boudin, B. Rondot, M. Da Cunha Belo, Corros. Sci. 37 (1995) 1809.